



LABORATORI NAZIONALI DI FRASCATI

SIS – Pubblicazioni

LNF-96/069 (P)
29 Novembre 1996

The DAΦNE Physics Program

Juliet Lee-Franzini

INFN – Laboratori Nazionali di Frascati, P.O. Box 13, I-00044 Frascati (Rome), Italy

Abstract

The physics program of DAΦNE is described in this article, as is the general purpose detector KLOE. The current status of KLOE is also briefly summarized.

1 KLOE'S Physics Program

1.1 *CP* and *CPT* by quantum interferometry

Consider the process $\phi \rightarrow K\bar{K} \rightarrow f_1, t_1 + f_2, t_2$ where a K^0 meson decays into a state f_1 at time t_1 and the other into a state f_2 at time t_2 , as illustrated below.



The decay intensity to f_1, f_2 , as a function of $\Delta t = t_1 - t_2$ and for $\Delta t > 0$, is:

$$I(f_1, f_2; \Delta t) = \frac{1}{2\Gamma} |\langle f_1 | K_S \rangle \langle f_2 | K_S \rangle|^2 \left(|\eta_1|^2 e^{-\Gamma_L \Delta t} + |\eta_2|^2 e^{-\Gamma_S \Delta t} - 2|\eta_1||\eta_2| e^{-\Gamma \Delta t / 2} \cos(\Delta m \Delta t + \phi_1 - \phi_2) \right)$$

where $\eta_i = \langle f_i | K_L \rangle / \langle f_i | K_S \rangle$ and a similar expression holds for $\Delta t < 0$. The interference term is sensitive to Δm , the magnitudes of the amplitude ratios

PACS.: 11.30.Er, 13.20.Eb, 13.20.Jf, 29.40.Vj

To be published on Frascati Physics Series

η 's and their phase difference, while the complete distribution depends also on the K_S and K_L lifetimes. One can thus perform a whole spectrum of precision “kaon-interferometry” experiments at DAΦNE by measuring the above decay intensity distributions for appropriate choices of the final states f_1, f_2 . Four examples are listed below.

1. With $f_1=f_2$ one measures Γ_S, Γ_L and Δm , since all phases cancel. Rates can be measured to $\times 10$ improvement in accuracy and Δm to $\times 2$.
2. With $f_1=\pi^+\pi^-, f_2=\pi^0\pi^0$, one measures $\Re(\epsilon'/\epsilon)$ at large time differences, and $\Im(\epsilon'/\epsilon)$ for $|\Delta t| \leq 5\tau_s$. Fig. 1(a) shows the interference pattern for this case.
3. With $f_1 = \pi^+\ell^-\nu$ and $f_2 = \pi^-\ell^+\nu$, one can measure the CPT -violation parameter δ_K ¹⁾: its real part at large time differences and the imaginary part for $|\Delta t| \leq 10\tau_s$. Fig. 1(b) shows the interference pattern.
4. For $f_1 = 2\pi, f_2 = \pi^+\ell^-\nu$ or $\pi^-\ell^+\nu$ small time differences yield $\Delta m, |\eta_{\pi\pi}|$ and $\phi_{\pi\pi}$, while at large time differences, the asymmetry in K_L semileptonic decays provides tests of T and CPT . The *vacuum regeneration* interference is shown in fig. 1(c).

In all, by choosing appropriate f_1 and f_2 channels one can determine 16 independent parameters describing the neutral K system. If the validity of the $\Delta S = \Delta Q$ rule is assumed there are only 13 parameters to be determined. Experiments at DAΦNE can thus test CPT invariance, in addition to studying CP violation. Should however the $\Delta S = \Delta Q$ rule not hold (it is expected to be violated to only one part in 10^7 in the Standard Model), there are in fact 17 independent parameters ²⁾. Therefore we will need to use strangeness tagged K^0 's, which can be obtained from charge exchange of K^+ mesons, in turn tagged by observation of a K^- meson from the copious decay $\phi \rightarrow K^\pm$.

1.2 Measuring $\mathcal{R}^\pm/\mathcal{R}^0$

We can also use the classical method of the double ratio $\mathcal{R}^\pm/\mathcal{R}^0 = 1 + 6 \times \Re(\epsilon'/\epsilon)$, and other ways of measuring $\Re(\epsilon'/\epsilon)$ from selected final states. Very different systematics are involved, thus allowing a self-check of the results. In fact, one can illustrate the statistical accuracy achievable at DAΦNE easily using the double ratio method (recall that the tagging efficiency drops out identically here and thus do not contribute to systematic errors).

In abbreviated form, the double ratio is

$$\mathcal{R}^\pm/\mathcal{R}^0 = \frac{N_L^\pm/N_S^\pm}{N_L^0/N_S^0} \approx 1 + 6\text{Re}\frac{\epsilon'}{\epsilon},$$

where each N refers to the number of $K_{L,S}$ decaying to two charged or neutral pions. The N_S numbers will evidently be much larger than the N_L ; thus, the statistical

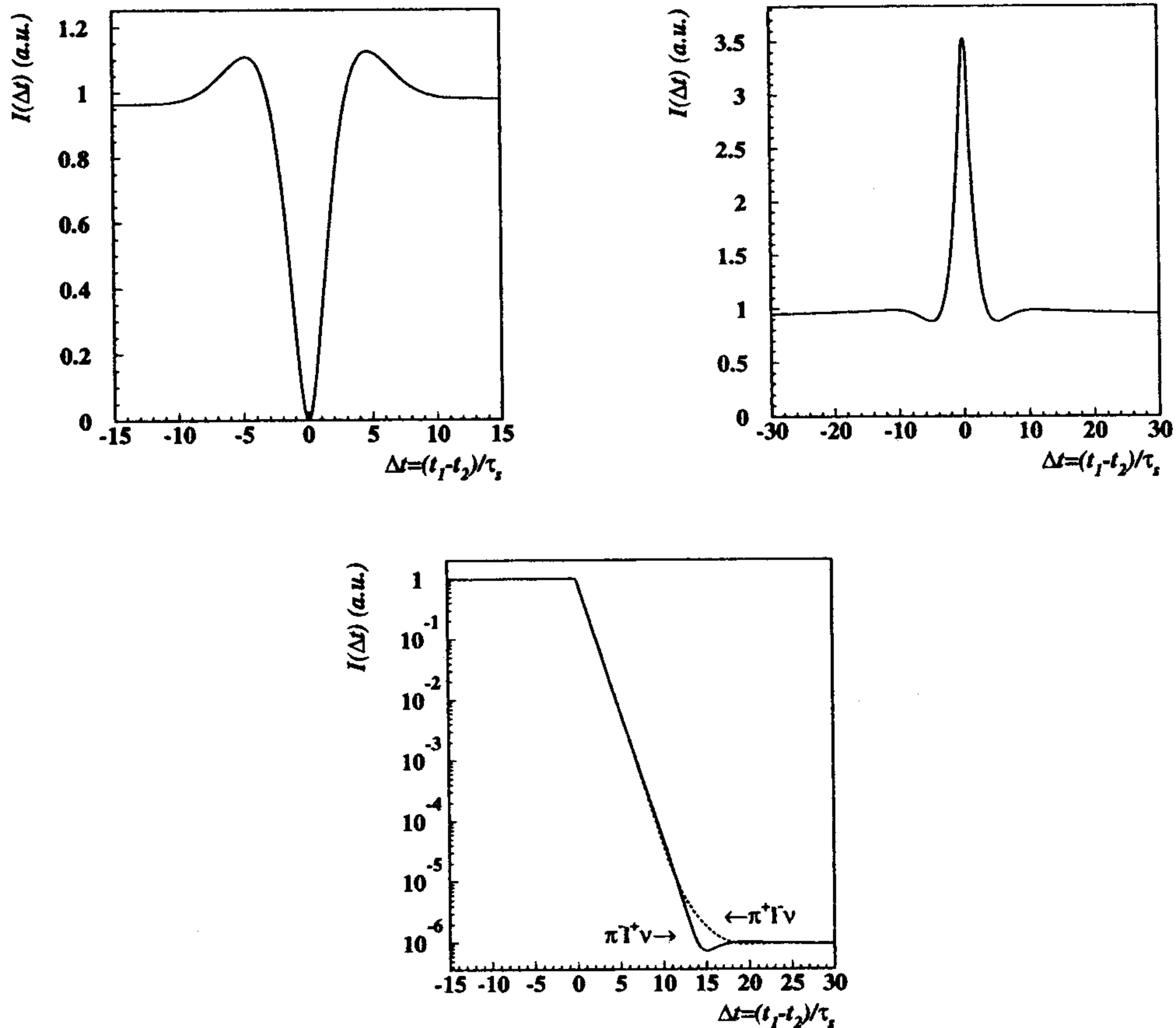


Figure 1: (a) Interference for $f_1 = \pi^+ \pi^-$, $f_2 = \pi^0 \pi^0$. (b) Interference for $f_1 = \ell^-$, $f_2 = \ell^+$. (c) Interference pattern for $f_1 = 2\pi$, $f_2 = \ell^\pm$.

errors coming from them will be negligible compared to those coming from the N_L . We thus have

$$\delta \left(\frac{\epsilon'}{\epsilon} \right) = \frac{1}{6} \sqrt{(\Delta N_L^\pm)^2 + (\Delta N_L^0)^2} = \frac{1}{6} \sqrt{\frac{1}{N_L^\pm} + \frac{1}{N_L^0}} = \frac{1}{6} \sqrt{\frac{3}{2N_L^0}},$$

since by isospin symmetry there are twice as many charged two-pion decays as neutral two pion decays. N_L^0 is given by the ϕ cross-section, times the integrated luminosity per year, times the efficiency for K_L tags, times $BR(\phi \rightarrow K_L K_S)$, times $BR(K_L \rightarrow \pi^0 \pi^0)$, times the number of K_L 's that are within the fiducial volume (i.e., that are detectable):

$$N_L^0 = 5 \mu b \times 10^{10} \mu b^{-1} \times 2/3 \times 0.34 \times 10^{-3} \times (1 - e^{-150/350}) = 4 \times 10^6,$$

which gives as claimed,

$$\delta \left(\frac{\epsilon'}{\epsilon} \right) = 1 \times 10^{-4}.$$

1.3 Other CP violating process/decays

So far CP violation has only been seen in K_L decays ($K_L \rightarrow \pi\pi$ and semileptonic decays). DAΦNE can look for $K_S \rightarrow \pi^0\pi^0\pi^0$, the counterpart to $K_L \rightarrow \pi\pi$. The branching ratio for this process is proportional to $\epsilon + \epsilon'_{000}$ where ϵ'_{000} is a quantity similar to ϵ' , signalling direct CP violation. It is not as suppressed as the normal ϵ' , perhaps a factor of twenty less. Nonetheless, as the expected BR is 2×10^{-9} , the whole signal will be at the 30 event level, and therefore there is here only the possibility to see the CP impurity of K_S , never observed before, not direct CP violation. The current limit on this BR is 3.7×10^{-5} . Another possibility is to look at the difference in rates between $K_S \rightarrow \pi^+l^-\nu$ and $K_S \rightarrow \pi^-l^+\nu$, which is expected to be $\sim 16 \times 10^{-4}$, measurable in one year's running at DAΦNE, to an accuracy of $\sim 4 \times 10^{-4}$. Again this would be only a measurement of ϵ , not ϵ' , but the observation for the first time of CP violation in two new channels of K_S decay would be nonetheless of considerable interest.

Evidence for direct CP violation can be also be obtained from the decays of charged kaons which are copiously produced at DAΦNE. CP invariance requires equality of the partial rates for $K^\pm \rightarrow \pi^\pm\pi^+\pi^-$ (τ^\pm) and for $K^\pm \rightarrow \pi^\pm\pi^0\pi^0$ (τ'^\pm). One can improve the present rate asymmetry measurements by two orders of magnitude. One can also observe differences in the Dalitz plot distributions for K^+ and K^- decays in both the τ and τ' modes; at DAΦNE one could reach sensitivities of $\sim 10^{-4}$. Finally, differences in rates in the radiative two pion decays of K^\pm , $K^\pm \rightarrow \pi^\pm\pi^0\gamma$, are also proof of direct CP violation. At DAΦNE the sensitivity reachable is $\sim 1.4 \times 10^{-3}$.

1.4 Chiral perturbation theory

In the last decade chiral perturbation theory (CHPT) has been extended to the next order terms in the chiral expansion ($\mathcal{O}(m^4)$, $\mathcal{O}(p^4)$, $\mathcal{O}(m^2p^2)$). Many new amplitudes can then be predicted³⁾. At lowest order the CHPT relation predicts the slope of the scalar form factor, λ_0 . There is at present disagreement of experiment with the CHPT prediction, 0.017 ± 0.004 . One can measure λ_0 for K_L to an accuracy of 1.4×10^{-5} . Similar accuracies are obtainable for K^\pm and for λ_+ . There is only one measurement of the relevant $K_{\ell 4}$ form factors. These decays provide an unique opportunity for the determination of the $\pi\pi$ phase shift⁴⁾. The amplitudes for $K_{\ell 2,\gamma}$, $K_{\ell 2,e^+e^-}$ and $K_{\ell 3,\gamma}$ depend on the K charge radius. The rate for $K^\pm \rightarrow \pi^\pm\gamma\gamma$ and the $\gamma\gamma$ distributions are uniquely predicted by the chiral lagrangian approach. Dalitz decays of K mesons and two photon production of pions are also of great interest.

1.5 Radiative ϕ decays

Many other physics topics can be studied, especially at the DAΦNE start-up time, when the number of beam bunches will be approximately a quarter (30) of the

final design value. An example is the study of light meson spectroscopy. Precise measurements of the $\eta - \eta'$ mixing have important bearings on quark models and QCD, in particular on the question of whether there are gluonic components in the η and η' wave functions⁵⁾. In this regard, measurements of the radiative ϕ decays to η and to η' , which are feasible with great sensitivity using KLOE, can lead to a really decisive test, when combined with the information coming from other sources such as the analogous J/Ψ decays and the two-photon decays of η and η' . To complete the determination of the η' parameters we need measurements of the rare transition $\phi \rightarrow \eta'\gamma$. There is some room for a non-vanishing gluonic component in the η' . To give an idea of the expected order of magnitude of the branching ratio, for no gluonium in the η' and a mixing angle of 20° we expect $\text{BR}(\phi \rightarrow \eta'\gamma) \sim 1.2 \times 10^{-4}$. A Monte Carlo study⁶⁾ shows that KLOE can reach, during the commissioning year of DAΦNE, BR's of $\sim 10^{-6}$.

At the end of 1997, DAΦNE will begin delivering of the order of 500 ϕ -mesons/sec. This provides a unique opportunity to study the $f_0(975)$ in ϕ radiative decays, even for branching ratios which in some estimates could be as low as 1×10^{-6} . The unique, lightest scalar meson state $f_0(975)$ is poorly described by current models. By Monte Carlo studies we show that the branching ratio above can easily be measured in the neutral decay channel $f_0 \rightarrow \pi^0\pi^0$ ⁷⁾. In decays to $\pi^+\pi^-$, there are backgrounds from continuum processes⁸⁾. Interference between one of these processes and the f_0 amplitude leads to very interesting and complex patterns⁹⁾. A complete study of the photon spectrum from $e^+e^- \rightarrow \pi^+\pi^-\gamma$ at the ϕ peak, after suppression of continuum contributions by suitable kinematics and angular cuts, can determine the sign of the $\phi f_0\gamma$ coupling even for the smallest branching ratio, thus providing a totally new piece of information for the investigation of the nature of the f_0 ⁷⁾.

1.6 e^+e^- annihilations into hadrons from threshold to 1.5 GeV

Precise measurements of $\sigma(e^+e^- \rightarrow \text{hadrons})$ up to energies of ~ 1.5 GeV are necessary for the calculation of the muon anomaly a_μ ¹⁰⁾. The required accuracy for the measurements¹¹⁾ of $\sigma(e^+e^- \rightarrow \text{hadrons})$ is $\sim 0.5\%$, readily accessible to KLOE.

1.7 Other decays

DAΦNE will be a unique source of pure K_S , thanks to tagging, providing up to 10^{10} kaons per year, and allowing measurements of rare K_S decay modes, most of which have not been measured yet, down to the 10^{-8} or 10^{-9} level. Rare charged K decay modes will also be studied. It will be a place to study many rare decays, such as $\phi \rightarrow \eta\gamma$, and η decays. In table 1 some of the improvements that may be made in rare decay BR limits are listed.

Decay mode	To date	Limits that can be achieved at DAΦNE
$\eta \rightarrow 3\gamma$	$\text{BR} < 5 \times 10^{-4}$	1.4×10^{-8}
$\eta \rightarrow \omega\gamma$	$\text{BR} < 5 \times 10^{-2}$	10^{-9}
$\phi \rightarrow \rho\gamma$	$\text{BR} < 2 \times 10^{-2}$	10^{-9}
$\phi \rightarrow \pi^+\pi^-\gamma$	$\text{BR} < 7 \times 10^{-3}$	10^{-9}
$\eta \rightarrow \pi^0 e^+ e^-$	$\text{BR} < 4 \times 10^{-5}$	1.4×10^{-8}
$\eta \rightarrow \pi^0 \mu^+ \mu^-$	$\text{BR} < 5 \times 10^{-6}$	1.4×10^{-8}

Table 1: Rare decays.

2 FINUDA's Physics Program

DAΦNE is a unique copious source of tagged, low energy (16 MeV), monochromatic charged kaons, which can be stopped in a very thin target, offering the possibility of a unique nuclear physics program:

1. Spectroscopy of Λ -hypernuclei.
2. Decays of Hypernuclei, $\Delta I \neq 1/2$
3. Do Σ -hypernuclei exist?
4. Search for exotic states.

The FINUDA collaboration is composed of INFN university sections of Bari, Brescia, Pavia, Torino, Trieste; the Laboratori Nazionali di Frascati dell'INFN, Frascati, plus Canadian and Iranian collaborators. The FINUDA detector ²³⁾ is a non focusing magnetic spectrometer with cylindrical geometry. It consists of a central interaction/target region which is composed of 1.5 mm thick scintillators (TOFINO) surrounding a thin beam pipe, two 300 μm silicon microstrip arrays (ISIM and OSIM) sandwich a 1.5 mm carbon target; an external tracking system consisting of two arrays of eight planar drift chambers and an array of straw tubes; finally surrounded by an outer scintillator array (TOFONE). The full apparatus is immersed in a solenoidal field of 1.1 Tesla. The position information from the ISIM allow the reconstruction of the kaon tracks, which together with the hypernuclear formation pion's trajectory obtained from the outer tracking system, allows the determination of the K^- in the stopping target. The fast scintillators are used for a first level trigger, allowing a topology selection of back to back events K^+ and K^- from ϕ decays). The TOFONE also serve as the neutron detectors for FINUDA, which will be situated in the second interaction region of DAΦNE and is due to be operational late 1997.

3 DEAR's Physics Program

An international collaboration constituted by 11 institutions from six countries ²⁴⁾ have designed an atomic physics experiment to be run as soon as electron and positrons will be circulating in DAΦNE, in the DAY-ONE configuration of the interaction regions. The aim of DEAR is to determine the K-nucleon scattering length by measuring the X-ray transitions in the kaonic hydrogen. They use the low momentum, monochromatic, high purity "kaon beam" from the ϕ 's produced at DAΦNE, impinging on a pressurized, low temperature, gaseous hydrogen target of moderate density, to reduce the Stark mixing effect. They use a Charged Coupled Device as detector, which is at present the best detector for soft X-rays in terms of background rejection and resolution.

4 The KLOE Design

The KLOE-Detector was proposed to the LNF's Scientific committee and given stage-I approval April 28, 1992 ¹²⁾. A technical design proposal was submitted to the same committee on January 12, 1993 ¹³⁾ and it was fully approved on March 19, 1993. Three additional addenda were written to amplify design concerns specific to the central drift chamber ¹⁴⁾, the data acquisition system ¹⁵⁾ and the trigger system ¹⁶⁾. These five documents by the KLOE Collaboration are the source materials containing the full evolutionary details of the KLOE design. Here, I have extracted the salient features and the parameters of the main components of the final detector. I also list some of the interesting results obtained during our prototyping and test work, to give a flavor of how much has been achieved and what still remains to be done.

The KLOE detector requirements are:

1. Collect enough statistics
2. Measure the path length of the K_S , K_L decays to the required accuracy
3. Reject backgrounds at the desired level
4. Be self-calibrating, using various K decay modes, in addition to Bhabha scattering events.

Its scale is driven by a fundamental parameter, the mean decay path length of the long lived K^0 -meson $L(K_L)$: at DAΦNE, $\beta(K)=0.216$ and $L(K_L) = \gamma\beta c\tau = 3.44$ m.

4.1 The KLOE Collaboration

The KLOE Collaboration has approximately 140 members from 10 Italian institutions supported by the INFN: Bari, Frascati, Lecce, Napoli, Pisa, Roma I, Roma

II, Roma III, ISS Roma, Trieste/Udine, four foreign ones: IHEP at Beijing, Univ. of Karlsruhe, Columbia Univ. and SUNY at Stony Brook. The individual name rosters are in references (12, 13, 14, 15, 13). The spokesman since its inception is Paolo Franzini.

4.2 Systematics constraints

Since the observation¹⁷⁾ in 1964 that the long lived K^0 meson decays into two pions, the search for direct CP violation has failed. In terms of physical observables, if the direct CP violating amplitude $\langle \pi\pi | K_2 \rangle$, where K_2 is CP -odd, vanishes, then:

$$\mathcal{R}_S \equiv \frac{\Gamma(K_S \rightarrow \pi^+\pi^-)}{\Gamma(K_S \rightarrow \pi^0\pi^0)} = \mathcal{R}_L \equiv \frac{\Gamma(K_L \rightarrow \pi^+\pi^-)}{\Gamma(K_L \rightarrow \pi^0\pi^0)},$$

otherwise, in general, $|\mathcal{R}_S - \mathcal{R}_L| = \Delta\mathcal{R} \neq 0$ and $|\Delta\mathcal{R}/\mathcal{R}| = 6 \times |Re(\epsilon'/\epsilon)|$.

The aim of KLOE is to reach a sensitivity in $\Delta\mathcal{R}/\mathcal{R}$ of $\sim 6 \times 10^{-4}$, which from the statistical point of view, is achievable at DAΦNE at full luminosity in about one year. The two formidable tasks for KLOE to face are the controlling of efficiencies for the decays of interest and the rejection of background from the copious K_L decays to states other than two pions. The relation between measurements and BR's, assuming tagging is used, is:

$$\underbrace{N_{L,S}^{\pm,0}}_{\text{observed}} - \underbrace{BK_{L,S}^{\pm,0}}_{\text{estimated}} = \underbrace{N_{KK} \times \varrho_{L,S}(\text{tag})}_{\text{cancels in ratio}} \times \underbrace{BR_{L,S}^{\pm,0}}_{\text{desired}} \times \underbrace{\langle \varrho_{L,S}^{\pm,0} \rangle}_{\text{efficiency}} \times \int_{\text{FV}} \int g(l-l') I(l) dl dl'.$$

The double integral is a convolution of the decay intensity $I(l)$ and the experimental resolution $g(l-l')$ in the measurement of the decay path length and an integration over the fiducial volume, FV, of the detector. The four backgrounds $BK_{L,S}^{\pm,0}$ and the averaged efficiencies $\langle \varrho_{L,S}^{\pm,0} \rangle$ are different. They must be known to an accuracy of $\mathcal{O}(1/3000)$.

4.3 Fiducial volumes

As will be described later, our detector consists of an electromagnetic calorimeter and a large tracking chamber. The calorimeter has a central part which is a cylinder of 2 m radius and 3.5 m length, closed by two end caps, covering $\sim 98\%$ of the solid angle. The chamber, with inner wall of 25 cm radius, provides tracking for $30 < r < 200$ cm. The whole detector is immersed in a solenoidal field of 0.6 T. Regeneration in walls (beam pipe, chamber walls) is $\leq 1\%$. Use of a large beam pipe, 10 cm radius, inside which all K_S 's decay, and rejection of K decays up to 6 cm ($10 \tau_S$) past any wall eliminate the effects of $K_L \rightarrow K_S$ regeneration. The fiducial volume (FV) for K_S and K_L decays are idealized in fig. 2. The fiducial volume for K_L decays, in cylindrical coordinates, is taken as:

$$30 < r < 175 \text{ cm} - 125 < z < 125 \text{ cm}.$$

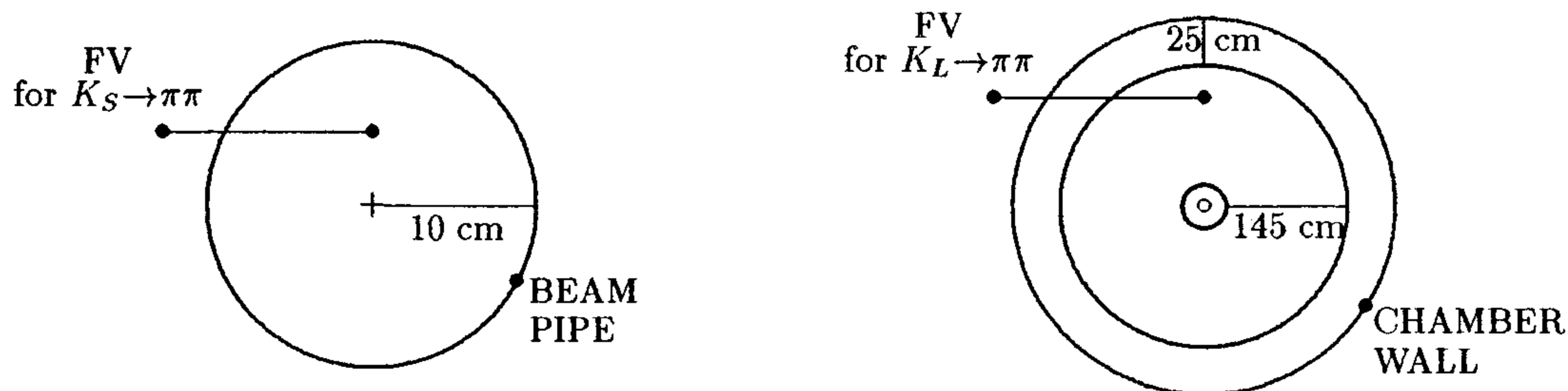


Figure 2: Fiducial Volumes for K_S and K_L decays.

If the integral over the FV equation could be carried out to infinity, FV boundary and resolution would not contribute any error. This is essentially the case for K_S decays. A K_L signal guarantees the presence of a K_S . The beam pipe has radius equivalent to ≥ 13 – 17 lifetimes. Therefore without imposing, ideally, any fiducial volume cut on the data, the integrals are “1”, independently of flight path resolution. Efficiencies for $\pi^+\pi^-$ and $\pi^0\pi^0$ decays are $\geq 99\%$ and are well-controlled. Backgrounds are at the level of 10^{-3} , before any cuts are applied.

The case is quite different for K_L decays, since the fiducial volume has dimensions, ~ 145 cm, which are about half the mean decay path of ~ 350 cm. A small error on the determination of the boundary of the fiducial volume can introduce large errors on \mathcal{R}_L , at the accuracy of interest. What is relevant is the relative error in the determination of the boundaries of the fiducial volumes for $K_L \rightarrow \pi^+\pi^-$ and $K_L \rightarrow \pi^0\pi^0$, since different methods are used to obtain the K_L path length. $K_L \rightarrow K_S$ regeneration at the chamber’s inner wall provides in fact an excellent check of the correct knowledge of the inner boundary of the fiducial volumes. To achieve a sensitivity of 6×10^{-4} in $\Delta\mathcal{R}/\mathcal{R}$, we must insure that the outer boundaries of the fiducial volumes for charged and neutral decays are equal to better than 0.5 mm. The most effective way to ensure this is to use K_L decays for which both a “neutral” and a “charged” decay vertex is measurable, such as $K_L \rightarrow \pi^+\pi^-\pi^0$. Decays of charged K ’s, $K^\pm \rightarrow \pi^\pm\pi^0$, can also be used over part of the FV.

4.4 Backgrounds

The main sources of background in CP experiments are the non- CP violating decays of K_L , $\pi^0\pi^0\pi^0$, $\pi^+\pi^-\pi^0$, $K_{\mu 3}$, and $K_{e 3}$, ~ 100 times more abundant than the CP -violating modes. The rejection of $\pi^0\pi^0\pi^0$ relies on good solid angle coverage and efficiency for γ ’s down to 20 MeV energy, which we will achieve in correct calorimeter design. The rejection of $\pi^+\pi^-\pi^0$ is easier because the probability of losing 2/2 γ ’s is 15 times smaller than losing 2/6 γ ’s; in addition, we will have help from chamber measurements of the charged tracks.

A realistic study of the methods for removing $K_{\mu 3}$ contamination has been developed. A large sample, 1.35×10^7 $K_{\mu 3}$ and 10^5 $K_L \rightarrow \pi^+\pi^-$ events, was gener-

Parameter	Method, Process	Accuracy/m
Energy Scale	Continuous, absolute: BHABHA	1%/cluster
Time Scale	– same – : BHABHA	12ps/cluster
Tracking Efficiency	– same – : e^+e^- , $\mu^+\mu^-$, $K \rightarrow 3\text{body}$	10^{-3} /track
Photon Efficiency	– same – : $K^\pm \rightarrow \pi^\pm\pi^0$, $K^0 \rightarrow \pi^+\pi^-\pi^0$	10^{-3} /cluster
F.V. $\pi^0\pi^0/\pi^+\pi^-$	Cont., relative: $K^\pm \rightarrow \pi^\pm\pi^0$, $K^0 \rightarrow \pi^+\pi^-\pi^0$	10^{-3} /global

Table 2: Detector Calibration

ated using the standard size of the luminous region, $\sigma_x = 0.2$ cm, $\sigma_y = 20$ μm , $\sigma_z = 3$ cm. $K \rightarrow K_{\mu 3}$ and $K \rightarrow \pi^+\pi^-$ events are distinguished by the use of a χ^2 function constructed using the measured variables corresponding to all the kinematical constraints available. A double Gaussian parameterization has been applied to the resolution functions (in p_T , ϕ , $\cot(\theta)$, vertex position) obtained from reconstructed GEANFI¹⁸⁾ generated tracks, using the ARGUS-KLOE program for a 84 layer stereo chamber, to take tails into account. The χ^2 function is peaked at very low values for $K_L \rightarrow \pi^+\pi^-$ decays, while for $K_{\mu 3}$ events it vanishes at 0 and extends to very high values. This calculation has been repeated for several values of the magnetic field, 4 to 8 kG. The rejection factor at 6 kG is approximately 4.5×10^{-4} with a $\pi^+\pi^-$ signal efficiency of 98.8%¹⁴⁾. The $K_{e 3}$ decays are more easily distinguished and removed, partly because $m_e \ll m_\mu$, and the energy deposition pattern of an electromagnetic shower in the calorimeter is very distinctive.

4.5 Calibration

At DAΦNE a general purpose detector capable of measuring all decay modes of the ϕ has a wealth of processes useful for the calibration of its efficiencies. Furthermore the availability of abundant Bhabha scatterings observed in the detector allows a complete calibration of energy and time scales. The following table summarizes the accuracies to which the key parameters can be monitored by various methods. We conclude that KLOE is truly a “self-calibrating” detector!

5 The KLOE Detector

From the discussions of the previous section we conclude that KLOE must be able to track charged particles of momenta between 50 and 250 MeV/c. It must also detect with very high efficiency γ 's with energy as low as 20 MeV, measure their energies with a resolution $\delta E_\gamma/E_\gamma \sim 15\%$ at 100 MeV, and provide the space coordinates of the photon conversion point so that the K_L decay path can be determined to within ~ 1 cm. Thus while the general features of the KLOE detector are similar to those of a *typical* general purpose collider's apparatus: a cylindrical structure surrounding

the beam pipe, consisting of a highly efficient, large tracking device for detecting the charged K^0 decay products, an electromagnetic calorimeter with exceptional timing ability, which also provides some particle identification, all enclosed in a solenoidal field, each component has its own unusual features. The KLOE cross section is shown in fig. 3. The radius of the beam pipe around the luminous point is 10 cm. This allows the definition of a fiducial region for K_S decays without complication from regeneration. The beam pipe is made of 0.5 mm thick beryllium to minimize multiple scattering, energy loss for charged kaons and regeneration. The enlargement of the beam pipe at the interaction point, is a technical challenge for DAΦNE because it could act as a free wheeling RF cavity, with all the attending problems. In figure 3 we also show that the low β insertion permanent magnets are mounted directly on the beam pipe, inside KLOE, another difficult technical problem to be solved.

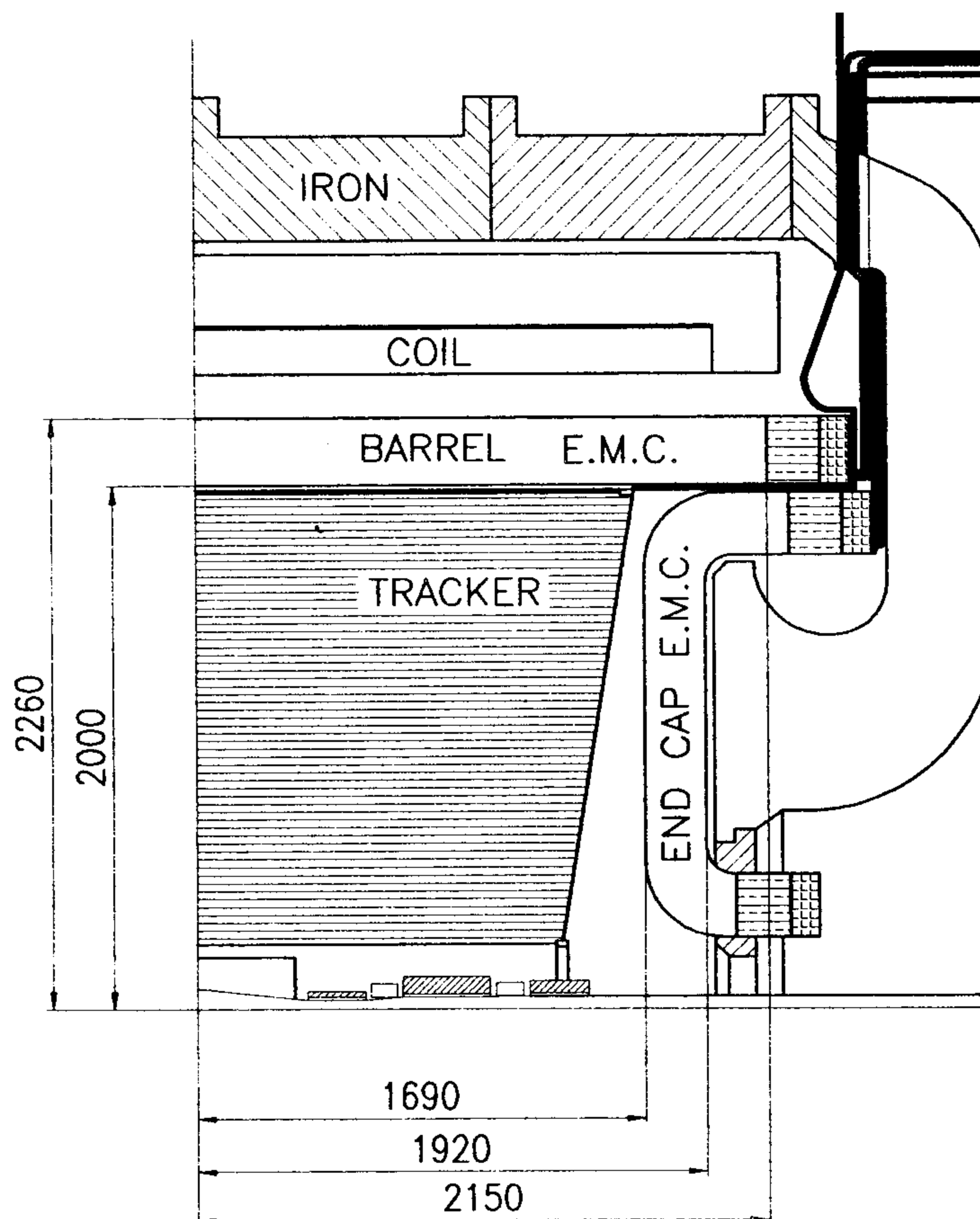


Figure 3: KLOE cross section along the beam axis.

5.1 Central Tracking Chamber

The design of the large tracking chamber for the KLOE detector is driven for the most part by the following considerations:

1. Maximize the homogeneity and isotropy of the active tracking volume because of the long decay path of the K_L and the isotropic angular distribution of the charged decay products.
2. Achieve a high and a well-controlled efficiency for the reconstruction of $K_L \rightarrow \pi^+ \pi^-$ decays.
3. Maximize, without forgetting the points above, the fiducial volume for decay detection, to obtain the largest event sample for a given delivered luminosity.
4. Optimize resolution at low momentum values.
5. Minimize the number of wires, both sense and field, in order to ease the difficulties of building a transparent chamber shell, minimize multiple scattering and maintain the electronics channels count within reasonable limits.

The decay length of K_L 's, $\lambda_D=350$ cm, requires that a long decay path be available to observe a significant fraction of their decays. A reasonable compromise is to detect K_L decays in a big, cylindrical chamber of radius ~ 2 m and length 370 cm. The above tracking volume is located inside a $15 X_0$ thick, lead-scintillating fiber e.m.calorimeter, surrounded in turn by a superconducting coil providing a solenoidal field of 0.6 T.

The quasi uniform distribution of K_L decay vertices and secondary tracks in the chamber volume requires a constant size drift cell. This is achieved by using only alternating stereo layers, with constant inward radial displacement at the chamber center, resulting in a stereo angle which increases with radius, in KLOE $50 \text{ mrad} \leq \theta_{st} \leq 120 \text{ mrad}$, and an approximately constant, square cell shape along z , with constant wire gain. An optimal configuration, assuring good tracking also for $K_S \rightarrow \pi^+ \pi^-$ decays consists of twelve layers in the inner part of the chamber with $1.5 \times 1.5 \text{ cm}^2$ cells, followed by 3×3 cells. The number of cell layers for this case is 61 for a total number of cells of $\sim 13,000$.

Because of the low momenta of the decay products, <300 MeV, we choose helium-based gas mixtures to minimize multiple scattering. A satisfactory choice is a 90-10 mixture of He-iC₄H₁₀ whose radiation length is $X_0=1300$ m. The wires, W for sense and Al for field, result in a final value $X_0=900$ m. Also, the choice of a relatively big drift cell of $3 \times 3 \text{ cm}^2$ helps in reducing the total amount of material in the chamber, while still maintaining a proper time-space correlation over most of the cell. Drift velocity is generally not saturated. For an expected resolution on any single measurement of $\sigma_{r\phi} \leq 200 \text{ } \mu\text{m}$, the $K_L \rightarrow \pi^+ \pi^-$ vertex is expected to be reconstructed with accuracies $\sigma_{x,y} \leq 500 \text{ } \mu\text{m}$, $\sigma_z \leq 1-2 \text{ mm}$. The resolution for the reconstructed K_L mass is $\sigma_M \sim 1 \text{ MeV}$. The low drift velocity of

Drift Chamber, He gas mix, thin walls	
$\delta point$	$= 200 \mu\text{m}, r \text{ and } \phi$
	$= 2 \text{ mm}, z$
δp_t	$= 0.5\% \times p_t$
$\delta(\tan(\theta))$	$= (3.5 \oplus 2.5) \times 10^{-4}$

Table 3: Central Chamber Performance.

He gas mixtures, and the smallness of the Lorentz angle, implies that the magnetic field will only change the time-space correlation without loss in either resolution or efficiency. This was confirmed during a beam test using a drift chamber prototype located inside a magnet, which could produce a field of 0.6 T, exposed to a beam at CERN. The effect of the magnetic field is measured to be small ($\simeq 5 \div 10\%$ change in drift velocity).

The KLOE chamber needs all its walls and attached apparatus to be as thin as possible in order to minimize photon conversions, multiple scattering and energy losses of charged particles before they enter the electromagnetic calorimeter. The end plates of the KLOE chamber are spherical, kept apart by twelve rods attached to an outer ring. The plate deformation under load is strongly helped by properly attaching the plate outer rim to a torsionally stiff ring. Gas seal is completed by twelve panels which will be mounted after chamber stringing and an inner cylinder is attached to the end plates via two rings at the center of the plates which also provide support for the low β insertion. Panels and inner cylinder carry no loads in our chamber design. The mechanical structure of the drift chamber, with spherical end plates, can withstand without deformation the tension of some 50,000 wires with good transparency ($\leq 0.1X_0$) to photons from π^0 decays, to be detected in the calorimeter. The chamber is being assembled at LNF, we estimate eight months of wire stringing for about 50,000 wires. It should be instrumented and inserted into the KLOE detector by the fall of 1997.

In order to acquire first hand experience about all problems concerning materials, stringing procedure, gas tightness, signal and HV, etc. we have built a full length sector. The prototype, built with carbon fiber plates furnished by STESALIT A. G. of Zullwil, Switzerland, is 3.2 m long with 1 m² end plates. Five hundred single sense wire square cells, 3cm by 3cm and 1.5cm by 1.5cm, arranged in thirty layers, are strung at stereo angles in the range 50-120 mrad between two conical shaped carbon fiber end-plates¹⁹⁾. Cosmic ray and beam test results confirm that it is invaluable for acquiring experience about all phases of the project.

The performance required of the KLOE tracking device is given in Table 3.

5.2 Calorimeter

Reconstruction of the $\pi^0\pi^0$ decay mode of a 110 MeV/c momentum K , the determination of its decay point and the efficient rejection of the three π^0 decays make designing the electromagnetic calorimeter, EmC, a most challenging project. Unique to the KLOE experiment, is the method of determining the flight path of K_L , the segment ID in fig. 4, by time measurements. I is the ϕ decay point, the direction of ID is given by $-p_{K_S}$, and A is the photon conversion apex in the calorimeter. As illustrated in fig. 4, the flight time measurements for even a single photon of the four from $\pi^0\pi^0$ allow the determination of the K_L decay path. The time of arrival of a photon gives the flight path of the K^0 to an accuracy $\delta l = \beta_K c \delta t \sim 6 \times 10^{-3} \text{ cm} \times \delta t(\text{ps})$. For a 510 MeV K^0 , that is for four photons with $\sum E_\gamma = 510 \text{ MeV}$, one expects a time resolution of $\sim 100 \text{ ps}$ and a path resolution of 0.6 cm. Observation of only three out of four photons still allows an over-constrained determination of both the K^0 mass and the flight path, using time, position and energy measurements.

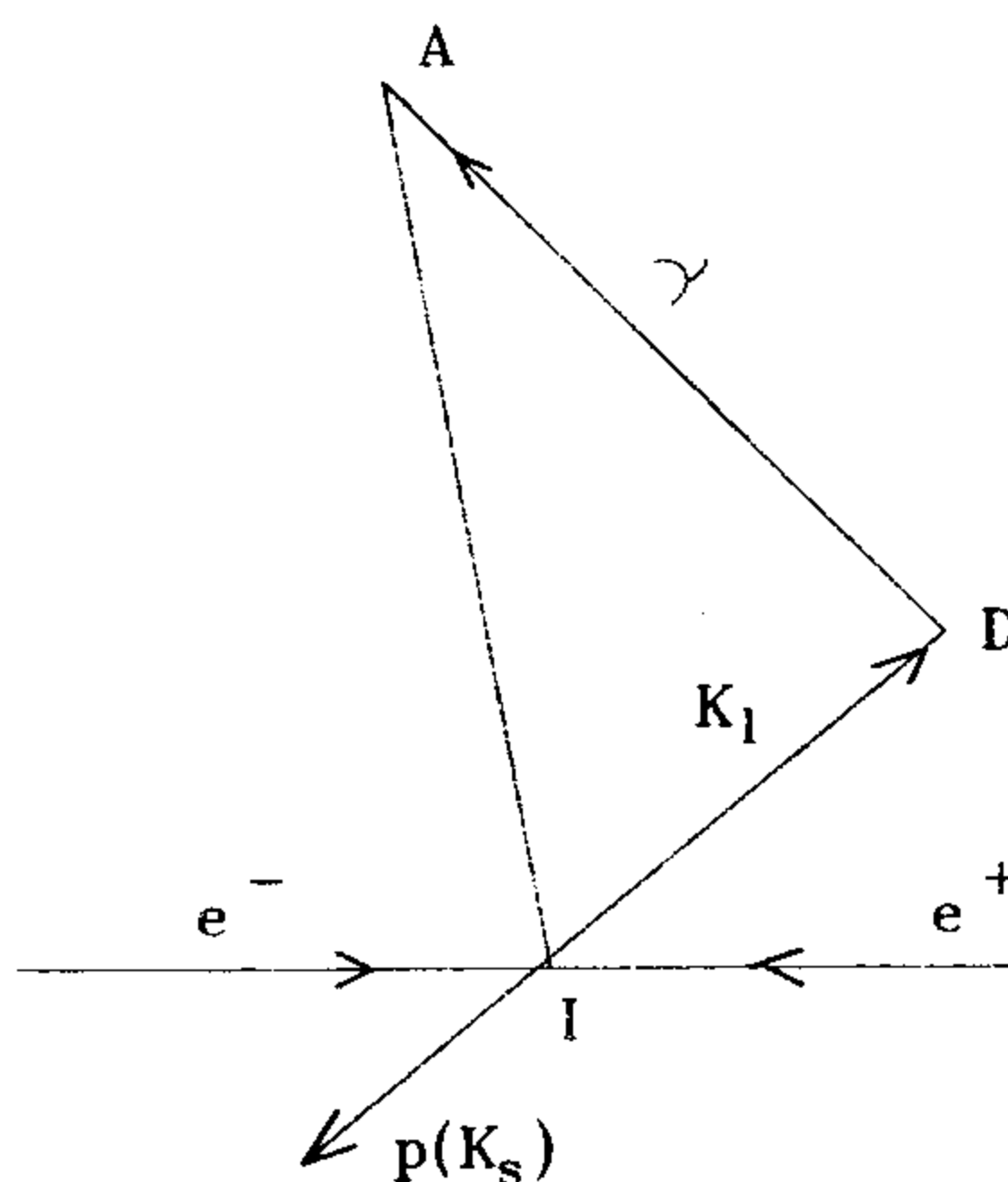


Figure 4: Measuring the K_L decay length.

The KLOE EmC is a very fine sampling lead-scintillating fiber calorimeter, with photomultipliers (PMs) read-out. The central part, barrel, approximates a cylindrical shell of 4 m inner diameter, 4.3 m active length and 23 cm thickness. The barrel covers the polar angle region $49^\circ < \theta < 131^\circ$ and consists of 24 sectors with trapezoidal cross section, $\sim 60 \text{ cm}$ wide. Two end-caps, 4 m in diameter and 23 cm thick, close hermetically the calorimeter. Each end-cap consists of 26 “C” shaped modules which run vertically along the chords of the circle inscribed in the barrel. At the two ends they are bent at 90° , becoming parallel to the barrel ends, to decrease the effects of the magnetic field on the PMs and to increase hermeticity, see figures 3 and 5. Partial KLOE views are shown in figure 5. The top figure shows an endview of the top half with half of the return iron yoke cut away, the lower figure shows a side view, again with half of the iron yoke cut away.

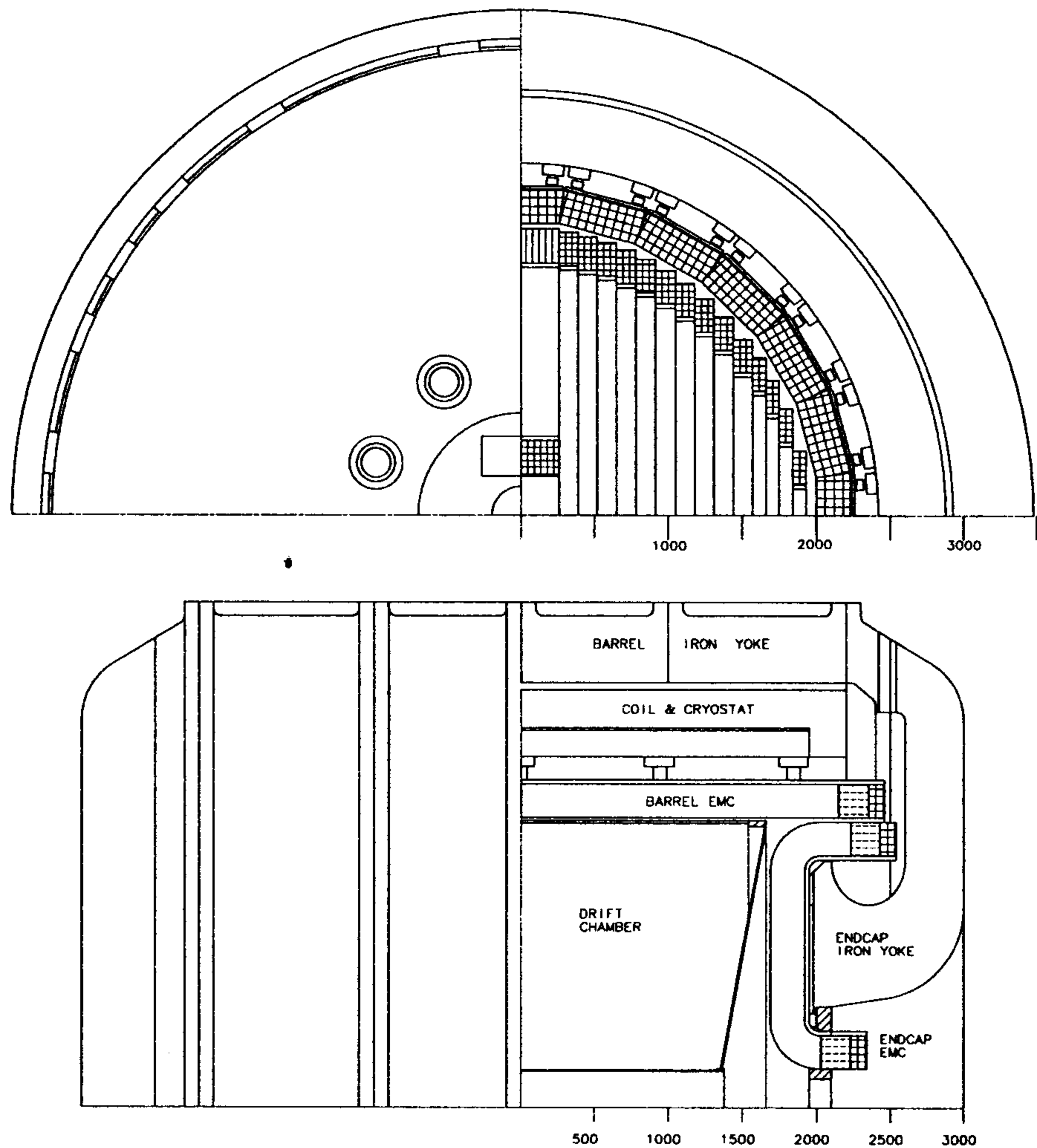


Figure 5: Partial KLOE views.

In our EmC fibers run mostly transversely to the particle trajectories. This reduces sampling fluctuations due to channeling, resulting in improved resolution particularly important at low energies. Each module of the KLOE EmC is built by glueing 1 mm diameter blue scintillating fibers between thin grooved lead plates, obtained by passing 0.5 mm thick lead foils through rollers of proper shape. The grooves in the two sides of the lead are displaced by one half of the pitch so that fibers are located at the corners of adjacent, quasi-equilateral triangles resulting in optimal uniformity of the final stack, see fig. 6. The grooves are just big enough to insure that the lead does not apply direct pressure on the fibers. Light travelling in the cladding is effectively removed because of the glue surrounding the fibers. The selected fiber pitch of 1.35 mm results in a structure which has a fiber:lead:glue volume ratio of 48:42:10 and a sampling fraction of $\sim 15\%$ for a minimum ionizing

particle. The final composite has a density of $\sim 5 \text{ g/cm}^3$ and a radiation length X_0 of $\sim 1.6 \text{ cm}$, is self-supporting, and can be easily machined. The very small lead foil thickness ($< 0.1 X_0$) results in a quasi-homogeneous structure and in high efficiency for low energy photons. Measurements indicate that the blue-green Kuraray SCSF-81, Bicron BCF-12 and Pol.Hi.Tech-46 fiber, satisfy our requirements for light yield, scintillation decay time and attenuation length²⁰⁾. Since the time resolution depends on the light yield, great care has been put in maximizing the efficiency of the light collection system and insuring uniform photocathode illumination. Each light guide consists of a mixing part and a Winston cone concentrator.²¹⁾ We are thus able to match the calorimeter elements to the PM photocathodes, with an area reduction factor of up to ~ 4 , without losses, because of the small 22° divergence angle of the light travelling in the fibers.

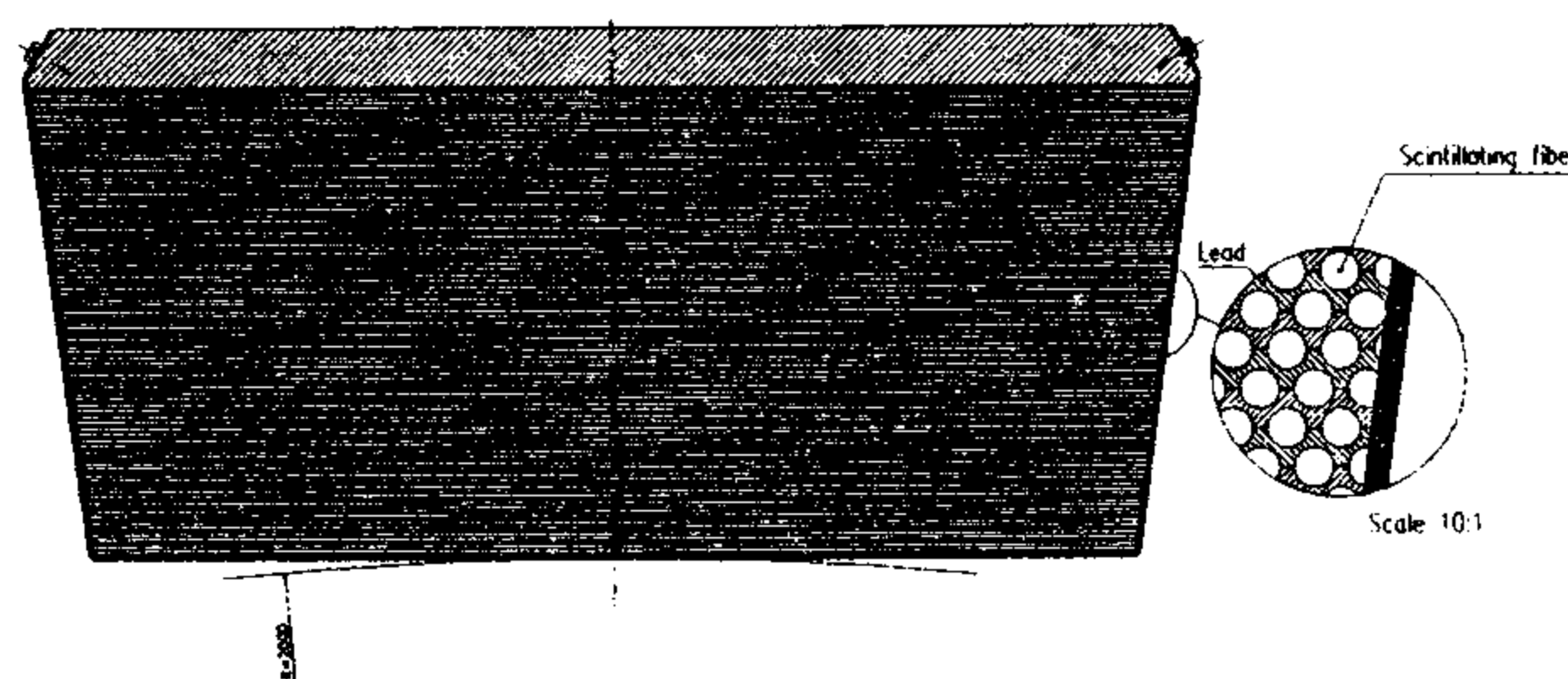


Figure 6: Fiber and lead layout.

All the machinery for building the *barrel* calorimeter have been designed and built by the KLOE calorimeter group, mostly at LNF. The first full size *barrel* module, with dimensions of $23 \text{ cm} \times 60 \text{ cm} \times 430 \text{ cm}$ and trapezoidal cross section, called module \emptyset , was then successfully built, also at Frascati. The machinery has been turned over to a company which constructed all modules of the *barrel* calorimeter. The front half of module \emptyset is built with Kuraray SCSF-81 fibers and the back half with Pol.Hi.Tech-46 fibers.

The module read-out consists of five planes of 12 elements each, of $\sim 4.4 \times 4.4 \text{ cm}^2$, varying slowly in size across the module face. Each element is viewed through light pipes which provide mixing and terminate with a Winston concentrator coupled to mesh photomultipliers. The PMs are manufactured to KLOE specifications by Hamamatsu (R2021, mod.). KLOE needs to use these special tubes because they can operate in moderate magnetic field. As shown in fig. 3, they are inside the return yoke where they see up to 0.15 T inclined less than 25° with respect to the PM's axis. These PMs have a measured quantum efficiency of only $\sim 60\%$ of the conventional tubes.

Module \emptyset employs the final KLOE electronics. The PM base contains the voltage divider for the PMs working with grounded cathode to allow grounding of

the tube shieldings and an A.C. coupled preamp which drives the cables carrying the signals outside of the magnet yoke. The signals enter three way splitters, providing input to a constant fraction discriminator, a driver for amplitude measurements and first level analog sums for trigger generation. All these functions are mounted on a 9U VME card, containing 30 complete channels. Signals from this card go to the KLOE designed 12 bit ADC's, $2 V \times 10$ ns full scale, and 12 bit TDC's, 25 ps per count. A description of KLOE electronics can be found in ref. 15).

Module \emptyset and subsequent modules were exposed to beams and cosmic rays. The results of the tests give $\sigma_E/E \sim 4.7\%/\sqrt{E (GeV)}$, $\sigma_T \sim 55ps/\sqrt{E (GeV)}$, and $\delta(Shower Apex) = 0.9$ cm. Aside from the measured energy and time resolutions quoted, we found the energy resolution to be independent of the incidence angle and we expect very little dependence of the time resolution on incidence. We have verified that the calorimeter can provide some added means to identify pions and muons.

5.3 Magnet

Of crucial importance in rejecting contamination of the $K_L \rightarrow \pi^+ \pi^-$ sample is the ability of performing good measurements of momenta in the range 155–268 MeV/c. In particular $K_{\mu 3}$ decays overlap kinematically $K_L \rightarrow \pi^+ \pi^-$ decays when the laboratory muon momentum is ~ 250 MeV. A simple argument predicts that kinematical overlaps decrease as the cube of the field value. This has been proved by full Monte Carlo calculations. A possible argument against high field is the loss of tracking efficiency and accuracy in vertexing for spiraling tracks. Again we barely see a loss in tracking efficiency beginning at 7 kG, $\sim 0.2\%$ as well as some saturation in the $K_{\mu 3}$ background rejection. This justifies our choice of 6 kG, which provides good rejection without impairing other detector functions. The chamber and calorimeter are inside a superconducting coil and the iron return yoke has deep cavities hollowed out so that the magnetic field therein is reduced and axial, to allow the proper functioning of the mesh photomultipliers employed in the EmC readout. Economical reasons, *i.e.*, power consumption, made us choose a superconducting coil. The coil was manufactured by Oxford Instruments and is scheduled to be delivered to Frascati in April, 1997.

5.4 Front-end Electronics

The KLOE detector contains 5,000 photomultipliers, PMs, for the readout of the calorimeter, and $\sim 13,000$ wires for the tracking chamber. The PM signals are amplified in the PMs' bases and sent to analog boards of 30 channels each. The outputs of this board are connected to ADCs, TDCs and to the trigger processor. The chamber signals are preamplified at the wire feed-through and sent to boards of 48 channels each. The output of two of these boards are connected to a 96 channel TDC board for drift time measurements. Module \emptyset tested to great satisfaction the following

chain of the final KLOE electronics at PSI in June 1994: PM bases containing the voltage divider and an A.C. coupled preamp which drives the cables carrying the signals to the outside, splitters which provide input to a constant fraction discriminator and to a driver for amplitude measurements, the KLOE designed 12 bit ADC's and 12 bit TDC's.

The TDC chips for the KLOE chamber digitization will reside in groups of three (96 channels) on modules fitting into the KLOE custom crates and readout scheme. Most of the functionality, digitization and event buffering, is integrated into a VLSI chip. The measurement of the signal drift-time coming from the chamber is performed by a custom integrated circuit, which is developed by the INFN Sezione di Roma1. The circuit is a multichannel common start/stop TDC, with 32 channels per chip. In KLOE the drift-time measurement is done by recording, for each signal, its time of arrival with respect to a stop signal, which is common to all channels and generated by the trigger. The TDC integrated circuit is developed as a full-custom device in 0.5 micron CMOS technology. Its working frequency is a function of an external reference clock that must be supplied to the circuit and it can be as high as 1 GHz (1 nsec LSB). The circuit is capable of detecting rising/falling edges, with a double edge resolution of 10 nsec or better. A programmable number of hits, from 1 to 16, can be stored for each channel. The hits are recorded as 16 bit words and every registered hit is stored in the chip for a programmable time interval. If during this time the chip does not receive a stop command the hit is removed, otherwise, the hit is kept for the read-out. The chip has also a multi-event buffering capability, 4 events deep, which is used only if at least one hit is present in one of the 32 channels, in a time window associated with a stop signal. Dedicated prompt trigger output lines inform the read-out of the presence in the chip of data to be read. The read-out of the data passes through the I/O port at a maximum speed of 50 MHz. The empty channels are automatically skipped during the read-out phase and for each registered hit the chip gives its absolute time value with respect to the stop signal and its channel number. Additional chip functions include an event counter, masking of the individual channels, and a self-test facility. The project has been successfully completed, we expect to mount the chamber electronics in the fall of 1997.

5.5 Trigger

At the full luminosity foreseen at DAΦNE ($10^{33} \text{ cm}^2\text{s}^{-1}$) the Φ event rate is $\simeq 5 \text{ KHz}$. The KLOE trigger must have extremely low inefficiency on these events ($\leq \text{few} \times 10^{-3}$) and reject/scale Bhabha, cosmic rays and machine background to acceptable rate. To do this task we designed a two level trigger based both on calorimeter and chamber information ¹⁶⁾.

Multiple energy deposits in calorimeter and/or high chamber multiplicity fires the first level trigger (pretrigger) within 150 ns from Φ decay. After 850 ns from the pretrigger a decision is taken using the other information gathered during this

time window. At maximum luminosity, rates of 20 and 10 KHz are foreseen ($\Phi +$ backgrounds) for level one and two respectively. Any signal conversion/digitization is performed within $2 \mu s$ from the Φ decay.

5.6 Data Acquisition

ϕ decays and calibration events represent, at full DAΦNE luminosity, a very large load for the data acquisition system. At 10,000 events per second, each event consisting of 2 to 4 kBytes, we estimate that 20,000 MIPS equivalent computing power will be necessary to digest the data. The universal approach appears to be farms of the new powerful μ -processors. We are looking at the α -VAX product of DEC, capable of 120 MIPS, amongst possible choices. We intend to write to tape all raw data, and we need to perform Monte Carlo simulations at the 10^8 , or greater, event level. The data produced in one year at full \mathcal{L} is $\sim 4 \times 10^{14}$ Bytes, to be stored at a bandwidth of 50–100 MBytes/s. The new Digital Linear Tapes, DLT by DEC, seems capable of such task. Due to the Monte Carlo simulation needs and the inevitable necessity of running production more than once we plan on two 20,000 MIPS farms. The major components of the KLOE DAQ system are briefly presented in the following ¹⁵⁾. Data comes from $\sim 25,000$ Front End Electronics channels housed in some 40 9U-VME crates. Signal conditioning and digitization is performed in a fixed time of $\mathcal{O}(2 \mu s)$, to avoid biases depending on event configuration. Every FEE channel contains buffers of appropriate depth, in order to eliminate data overflows and to allow asynchronous read-out. Data from the FEE are transferred to an on-line farm of Single Board Computers, SBC, using a two level concentration scheme. The first one is performed at crate level via a custom bus in the backplane, the AUXbus, and a hardwired read-out controller, ROCK, located in the crate itself. The ROCK implements the function of a sparse readout scanner collecting data related to each single trigger. The second level of concentration is performed by a ROCK manager, ROCKM, connected to chains of crates of suitable length with a cable bus, Cbus. Each ROCKM resides in a 6U-VME crate together with a VME processor which prepares sub-events for transmission to a given farm element. A commercial VME interconnector, VIC, connects all the crates in a chain allowing VME processors to program, check and debug FEE, ROCK's etc. The components of the DAQ system are interconnected via Ethernet for low bandwidth operations (controls, downloading, monitoring) and via FDDI for data transmission. A DEC FDDI GIGAswitch, with bridge functionality, is used to provide parallel paths between the VME processors and the farm in a scalable way. The number of switch ports dedicated to chains is chosen taking into account two factors: the maximum acceptable read-out ROCKM time and the throughput of the communication protocol achievable at VME and farm level. In order to improve the performance of the communication protocol, the sub-events related to the same group of consecutive trigger numbers are packed in sub-event-strings that must be gathered by a single SBC. The farm SBC's build and test the integrity of each event, implement the final

event formatting, and perform quality control on samples of the data. The address of each farm element is assigned by an additional VME processor, the data flow controller, DFC, connected also via VIC channels to the ROCKM crates. The DFC manages the load of all the VME processors, maintaining a table which maps groups of trigger numbers and SBC addresses. DAQ resets and buffer flush-out commands are generated when misalignment is detected at farm level. Other error conditions will be similarly handled. The farm is based on SBC's organized in crates. Each crate has a dedicated output SBC which manages the crate I/O to the storage devices. The total CPU power required for the whole farm is estimated to be about 16,000 Specint'92. CPU boards adequate for this are beginning to appear in the market. We wait for a final decision upon the outcome of a joint project between INFN and DEC designing a custom SBC using the DEC Alpha chip. A whole DAQ chain has been implemented and tested by November 1996.

5.7 Conclusions

The construction of the actual detector has been started at LNF. The orimeter modules has been already built and tested and assembly will end by the beginning of 1997. The central chamber is ready for stringing and will end by the fall of 1997. We foresee KLOE to be operational at beginning of the 1998.

6 Conclusions

The new facility DAΦNE to begin operation in December 1996, promises an era of precision and varied CP and CPT violation studies, together with a complementary program in particle and nuclear physics.

Acknowledgments

I wish to thank the HQ96 local organizers for their kind hospitalities. I wish to acknowledge and thank all my KLOE colleagues for their brilliant, wonderful and heroic efforts to realize KLOE. I also wish to thank C. Guaraldo for DEAR information and M. Betrani for FINUDA transparencies.

References

1. C. D. Buchanan *et al.*, Phys. Rev. **D45**, 4088 (1992).
2. L. Maiani, in “The DAΦNE Physics Handbook”, L. Maiani *et al.* Eds., Frascati, 1992, p. 21.
3. For all references on CHPT, see “The DAΦNE Physics Handbook”, ed. L. Maiani *et al.*, LNF, Frascati, 1992, p. 105-280.
4. M. Baillargeon and P. J. Franzini, in “The Second DAΦNE Physics Handbook”, eds L. Maiani, G. Pancheri and N. Paver, LNF Frascati, 1995, p. 413.
5. F. E. Close, in “The DAΦNE Physics Handbook”, L. Maiani *et al.* Eds., Frascati, 1992, p. 465.
6. J. Lee-Franzini, W. Kim, and P. J. Franzini, in “The DAΦNE Physics Handbook”, L. Maiani *et al.* Eds., Frascati, 1992 p. 533-534.
7. J. Lee-Franzini, W. Kim, and P. J. Franzini, Phys. Lett. **B287** 259 (1992); “The DAΦNE Physics Handbook”, Frascati, 1992, p. 513-544.
8. A. Bramon, G. Colangelo, P. J. Franzini and M. Greco, in “The DAΦNE Physics Handbook”, Frascati, 1992, p. 487.
9. P. J. Franzini and G. Colangelo, Phys. Lett. **B289**, 189 (1992).
10. T. Kinoshita, B. Nizić and Y. Okamoto, Phys. Rev. D **31**, 2108 (1985), and references therein; see in particular their reference 28.
11. P. Franzini, in “The Second DAΦNE Physics Handbook”, eds L. Maiani, G. Pancheri and N. Paver, LNF Frascati, 1995, p. 471.
12. “KLOE, A General Purpose Detector for DAΦNE”, the KLOE Collaboration, LNF Report LNF-92/019, April 1992.
13. “THE KLOE DETECTOR, *Technical Proposal.*” the KLOE Collaboration, LNF-93/002 (IR), January 1993.
14. “The KLOE Central Drift Chamber”, the KLOE Collaboration, LNF Report LNF-94/028, 1994.
15. “The KLOE Data Acquisition System”, the KLOE Collaboration, LNF Report LNF-95/014, 1995.
16. “The KLOE Trigger System”, the KLOE Collaboration, LNF Report LNF-96/043, 1996.

17. J. H. Christenson *et al.*, Phys. Rev. Lett. **13**, 138 (1964).
18. A. Antonelli, C. Bloise and A. Calcaterra, KLOE Notes 3, 23.
19. F. Grancagnolo, with the KLOE Chamber Group, NIM **RD9**, **367(1-3)**, 106 (1995).
20. A. Antonelli *et al.*, NIM **A370**, 367, (1996).
21. A. Antonelli *et al.*, NIM **A368**, 628, (1996).
22. A. Antonelli *et al.*, NIM **A354**, 352, (1995).
23. FINUDA, A Detector for Nuclear Physics at DAΦNE, the FINUDA Collaboration, LNF Report LNF-93/021, 1993.
24. DEAR, DAΦNE Exotic Atoms Research, the DEAR Propossal, DEAR Collaboration, LNF Report LNF-95/055, 1995.